velocities of 0.026 to 0.052 km s^{-1} at 230 GHz. Whenever possible, a frequency-switching mode was used.
5. The HPBW of the JCMT antenna is 14 arc sec at 345 GHz. Most data were obtained in the 300- to 370-GHz window with a spectral resolution of 95 kHz, in the frequency-switching mode.
6. N. Biver *et al.*, *Nature* **380**, 137 (1996).
7. Observations with the Nançay radio telescope (right ascension × declination of the HPBW was 3.5 arc min × 19 arc min) were undertaken with the technique previously used for comet P/Halley and other comets [E. Gérard, D. Bockelée-Morvan, G. Bourgois, P. Colom, J. Crovisier, *Astron. Astrophys. Suppl. Ser.* **77**, 278 (1989)].
8. A. Wootten *et al.*, *IAU Circular 6362* (1996); L. M. Woodney, J. McMullin, M. F. A'Hearn, *IAU Circular 6344* (1996); D. C. Lis *et al.*, in preparation; D. C. Lis *et al.*, *IAU Circular 6362* (1996).
9. H. A. Weaver *et al.*, *IAU Circular 6376* (1996).
10. J. Crovisier *et al.*, *Astron. Astrophys.* **315**, L385 (1996); J. Crovisier *et al.*, *Science* **275**, 1904 (1997).
11. J. K. Davies *et al.*, *Icarus*, in press.
12. A. Enzian, thesis, Université Joseph Fourier, Grenoble, France (1997).
13. One cannot yet exclude asymmetric collisional quenching (related to higher densities in the antisolar direction) as a contributor to the persistent blueshift observed for OH at $r_h < 2.5$ AU. Detailed modeling is needed to examine whether this effect is significant.
14. P. Eberhardt *et al.*, *Astron. Astrophys.* **187**, 481 (1987).
15. When the outgassing is isotropic, the width of the parent molecule radio line at half intensity is close to twice the gas expansion velocity. The lines observed in comet Hale-Bopp indicate preferential outgassing toward Earth. Hence, the outflow velocity can be only estimated from the blue wing of the profile.
16. D. Bockelée-Morvan, J. Crovisier, E. Gérard, *Astron. Astrophys.* **238**, 382 (1990). The OH ejection velocity was assumed to be 1.05 km s^{-1} [J. Crovisier, *ibid.* **213**, 459 (1989)].
17. F. P. Schloerb, W. M. Kinzel, D. A. Swade, W. M. Irvine, *Astron. Astrophys.* **187**, 475 (1987).
18. Molecule: model. OH: (*16*); linear molecules: J. Crovisier, *Astron. Astrophys. Suppl. Ser.* **68**, 223 (1987); CH_3OH: D. Bockelée-Morvan, J. Crovisier, P. Colom, D. Despois, *Astron. Astrophys.* **287**, 647 (1994); H_2S: J. Crovisier, D. Despois, D. Bockelée-Morvan, P. Colom, G. Paubert, *Icarus* **93**, 246 (1991); H_2CO: D. Bockelée-Morvan and J. Crovisier, *Astron. Astrophys.* **264**, 282 (1992). We assumed a total collisional cross section of 5×10^{-14} cm^2. A pure thermal model was used for CH_3CN.
19. The quenching radius r_q was estimated to have been $\sim 2.6 \times 10^5$ km in October and November 1996 at r_h = 2.2 to 2.7 AU, determined using the center exposure and the average east-west offset positions at 7 and 14 arc min, as in comet Hyakutake [E. Gérard *et al.*, in preparation]; the quenching was modeled according to $r_q = r_q^0 r_h (Q_{OH})^{0.5}$ [F. P. Schloerb, *Astrophys. J.* **332**, 524 (1988)], with r_q^0 = 40,000 km, r_h in astronomical units, and the OH production rate Q_{OH} in units of 10^{29} s^{-1}. We used the OH lifetime computed at solar minimum [S. A. Budzien, M. C. Festou, P. D. Feldman, *Icarus* **107**, 164 (1994)].
20. Haser molecular density distributions assume isotropic outflow at constant velocity. Production rates calculated with a more realistic angular density distribution are at most 15% higher.
21. The scale length of the H_2CO parent is assumed to be 1.2 times the photodissociative scale length of H_2CO, as measured in comet P/Halley [R. Meier, P. Eberhardt, D. Krankovsky, R. Hodges, *Astron. Astrophys.* **277**, 677 (1993)].
22. D. Jewitt, M. Senay, H. Matthews, *Science* **271**, 1110 (1996).
23. A. H. Delsemme, in *Comets*, L. L. Wilkening, Ed. (Univ. of Arizona Press, Tucson, AZ, 1982), pp. 85–130.
24. The H_2CO production rate computed under the assumption of direct release from the nucleus varies as $r_h^{-4.5}$. It is 0.2 to 0.7 times the H_2CO production rate computed by assuming an extended source.
25. W. M. Irvine *et al.*, *Nature* **382**, 418 (1996).
26. R. M. Lees, *Astrophys. J.* **184**, 763 (1973).
27. The interpretation of line shifts and the comparison of line shifts of different species observed with different fields of view must be done with caution because the molecular coma is generally resolved by the beam of the radio telescope, and a fraction of molecules with small projected velocities are not seen by the instrument. In the case of outgassing restricted to the hemisphere toward Earth, we estimated that the millimeter lines are more blueshifted than the OH lines by about 0.05 km s^{-1}. In the present study of the OH velocity shifts (Fig. 2A), we did not consider spectra obtained from September to mid-October 1996, which suffered from OH contamination from the galactic plane. The scatter in the H_2O expansion velocity (Fig. 2B) may be partly due to OH galactic contamination and the inability of the trapezium method to interpret asymmetric lines.
28. M. Womack *et al.*, *IAU Circular 6382* (1996); N. Biver *et al.*, *IAU Circular 6386* (1996).
29. D. Jewitt, M. Senay, H. Matthews, *IAU Circular 6377* (1996).
30. J. Crovisier *et al.*, *IAU Circular 6394* (1996).
31. L. M. Woodney *et al.*, *IAU Circular 6408* (1996).
32. N. Biver *et al.*, *IAU Circular 6421* (1996).
33. N. Biver *et al.*, *IAU Circular 6458* (1996).
34. D. Bockelée-Morvan *et al.*, *IAU Circular 6511* (1996).
35. The JCMT is operated by The Joint Astronomy Centre on behalf of the Particle Physics and Astronomy Research Council of the United Kingdom, the Netherlands Organisation for Scientific Research, and the National Research Council of Canada. The Nançay Radio Observatory is operated by the Unité Scientifique de Nançay of the Observatoire de Paris, associated as Unité de Service et de Recherche (USR) B704 to CNRS. The Nançay Observatory also gratefully acknowledges the financial support of the Conseil Régional of the Région Centre in France. This research has been supported by the Programme National de Planétologie de l'Institut National des Sciences de l'Univers and CNRS (URA 1757).

13 February 1997; accepted 6 March 1997

The Spectrum and Spatial Distribution of Cyanogen in Comet Hale-Bopp (C/1995 O1) at Large Heliocentric Distance

R. Mark Wagner* and David G. Schleicher

Optical spectra of comet Hale-Bopp (C/1995 O1) at a heliocentric distance of 6.45 astronomical units showed emission from cyanogen gas. The spatial distribution of cyanogen was considerably more diffuse and extended compared to the spatial profile of the dust or grains which were sharply peaked near the center. This behavior is consistent with comets at smaller heliocentric distances suggesting the same or a similar formation mechanism. A cyanogen gas production rate of (1.2 ± 0.3) $\times 10^{26}$ molecules per second was derived. A model band profile derived from fluorescence equilibrium calculations for the comet's heliocentric velocity and distance agrees with the observed band profile.

Comet Hale-Bopp (C/1995 O1) was discovered on 23 July 1995 at an integrated visual magnitude of ~11 (*1*) and at a heliocentric distance, r_h, of 7 astronomical units (AU) (*2*). The discovery of a luminous periodic comet at such a large distance from the sun initiated observations at optical and radio wavelengths to understand the physical and chemical processes occurring in the nucleus and coma which are not available from observations at smaller r_h. In particular, Fitzsimmons and Cartwright (*3*) detected emission from the CN (0-0) band in Hale-Bopp's coma at r_h = 6.82 AU; the second most distant reported detection for a comet (*4*, *5*).

Our observations of Hale-Bopp were obtained on 13.1 October 1995 universal time (UT) (r_h = 6.45 AU; 6.64 AU from Earth) with the 4.5-m Multiple Mirror Telescope and the blue channel charge-coupled device spectrograph (*6*). We obtained two 20-min exposures of Hale-Bopp with the spectrograph slit centered on the nucleus throughout the observation and oriented along the parallactic angle of 29° to minimize any loss of light due to atmospheric refraction. The position angle of the sun on the plane of the sky was 270° so that the slit was oriented nearly orthogonal to sun-tail direction on the sky. The spectrum of a solar analog star (van Bueren 64) was obtained to remove the reflected solar spectrum from the comet spectrum. The first comet exposure was heavily contaminated by background stars and was discarded.

The data were reduced and processed using standard procedures (*7*). Because any gas coma of Hale-Bopp is expected to be quite extended and probably even extends beyond the bounds of our short slit, sky subtraction was accomplished by first inter-

R. M. Wagner, Department of Astronomy, The Ohio State University, 174 West 18th Avenue, Columbus, OH 43210, USA, and Lowell Observatory, 1400 West Mars Hill Road, Flagstaff, AZ 86001, USA.
D. G. Schleicher, Lowell Observatory, 1400 West Mars Hill Road, Flagstaff, AZ 86001, USA.

*To whom correspondence should be addressed. E-mail: rmw@lowell.edu

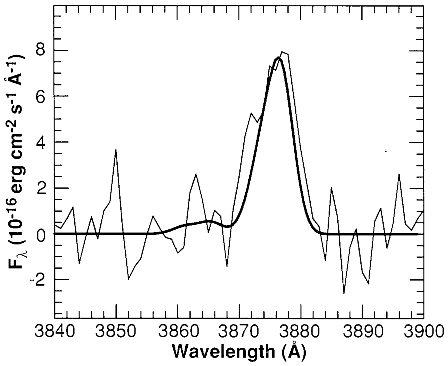

Fig. 1. Observed spectrum of Hale-Bopp showing the detection of CN ($\Delta v = 0$) in the coma (light curve). The heavy curve represents a model CN profile based on the results of fluorescence equilibrium calculations at an r_h of 6.45 AU (9) and scaled assuming our derived CN production rate.

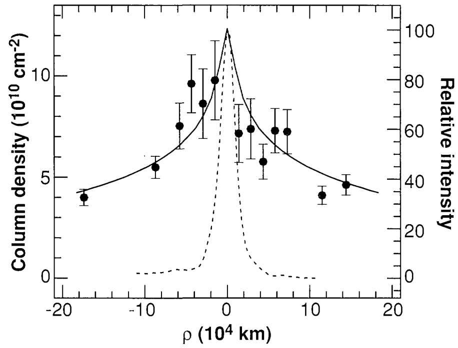

Fig. 2. The measured spatial distribution of CN in the coma of Hale-Bopp (solid circles) shown with their associated 1σ uncertainties. Comparison with the scaled Haser model (heavy curve) is also shown. The spatial profile of continuum which represents the distribution of the dust or grains in the coma is represented by the dashed curve.

polating across the emission band of CN at the extreme ends of the slit. We estimate that the error in our relative intensity calibration is less than about 7%. Based on the relative sizes of the seeing disk and the slit width and the resultant loss of standard star light, we estimate that the observed calibrated spectra of Hale-Bopp are on average a factor of 6 brighter than they would be in the absence of any standard star light losses.

We identified in the processed long slit spectrum, emission due to CN ($\Delta v = 0$) extending from the bright nuclear region and fading slowly to the ends of the slit in contrast to night-sky lines which cross the slit at constant intensity. To determine the spatial distribution of the CN emission, we extracted 14 individual spectra along the slit at locations free from stellar contamination. Each spectrum utilized a 5-arc-sec-long extraction aperture and we isolated the region surrounding CN ($\Delta v = 0$) between 3840 Å and 3900 Å for our analysis. To measure the flux of CN in each spectrum, the solar analog spectrum was scaled to match the background continuum of each spectrum and then subtracted. Our spectrum was formed by averaging the 14 individual spectra but excluding the spectrum centered directly on the bright nuclear condensation (Fig. 1). The observed average integrated band flux of CN ($\Delta v = 0$) is $(8.2 \pm 1.2) \times 10^{-15}$ erg cm^{-2} s^{-1}. Following a similar analysis, we failed to detect C_2 ($\Delta v = 0$) at 5000 to 5200 Å in the coma.

To determine the radial distribution of CN, we converted the measured integrated band fluxes to column densities (8) assuming that the fluorescence efficiency, *g*-factor $= 8.56 \times 10^{-15}$ erg s^{-1} molecule^{-1} at $r_h = 6.45$ AU (9) and the aperture diameter $\theta_s = 2.5$ arc sec (12,140 km at the comet), which is the diameter of the equivalent area circle corresponding to our 5 × 1 arc sec rectangular extraction aperture. The distribution of CN is very broad as compared to the dust or grains as measured by the spatial profile of gas-free continuum (Fig. 2). Such a broad distribution is expected, and typical of comets at small r_h, since CN is a daughter product of one or more parent molecules and also is believed to be released directly from grains (*10*). In each of these cases, CN is expected to have a much broader spatial distribution than the dust's canonical 1/ρ distribution, where ρ is the projected distance from the nucleus, due to the much higher nominal velocity of the CN molecules than of the dust grains. The agreement between the observed and Haser model spatial profiles of CN is surprisingly good, given that the Haser model parent and daughter scale lengths were derived from spatial profiles measured in comets having r_h between 0.7 and 1.5 AU and are scaled by r_h^2 (*11*). This suggests that these Haser model scale lengths for CN are well determined and are applicable over a wide range of r_h.

To determine the total production rate of CN, Q_{CN}, we fit the observed profile to a Haser model assuming fixed parent and daughter scale lengths of 1.3×10^4 $(r/1\ \mathrm{AU})^2$ and 2.1×10^5 $(r/1\ \mathrm{AU})^2$, respectively (*11*, *12*) (Fig. 2). We derived $Q_{CN} = (7.0 \pm 1.2) \times 10^{26}$ molecules per second from these data. Correction of the observed Q for light losses gives an actual $Q_{CN} = (1.2 \pm 0.3) \times 10^{26}$ molecules per second, where the uncertainty in Q is dominated by the uncertainty in the light-loss correction.

Using our measured Q_{CN}, we computed a model CN band profile to compare with the observed profile (Fig. 1). We used the results of fluorescence equilibrium calculations for CN ($\Delta v = 0$) at $r_h = 6.45$ AU and $v_h = -15.3$ km s^{-1} (9) and convolved with the instrumental resolution of 3.6 Å. The CN ($\Delta v = 0$) profile consists of the strong (0-0) band centered at 3876 Å and the weaker (1-1) band at 3864 Å (Fig. 1) and our calculations show that at $r_h = 6.45$ AU only eight rotational energy levels are populated, and therefore do not extend to the band head at 3883 to 3884 Å. Our computed profile had a total integrated CN ($\Delta v = 0$) band flux of 5.45×10^{-15} erg cm^{-2} s^{-1} and a position and shape in agreement with the observed profile. This is the first measurement of CN at large r_h with sufficient spectral resolution to test the CN fluorescence model (9) at a low level of solar radiation. Previous tests of the standard fluorescence model (*9*, *13*) were made for comets at $r_h \leq 1.3$ AU, or a level of solar radiation more than 25 times greater. Since the relative populations of CN molecules in the various rotational states depends on a balance between excitation of molecules by solar radiation and subsequent de-excitation with the emission of one or more photons, the relative line intensities within the emission band and the final fluorescence efficiency depends on the values of several de-excitation parameters. The agreement between the observed and theoretical profiles in Hale-Bopp (Fig. 1) indicates that the assumed values of these parameters are sufficiently accurate for analyses of CN observations obtained over a wide range of r_h.

Our spectroscopic observations confirm the detection of CN in the coma of Hale-Bopp at large r_h (*3*, *14*). Our derived production rate at 6.45 AU is comparable to their respective values for Q_{CN} of $(1.2 \pm 0.6) \times 10^{26}$ molecules per second and $(1.2 \pm 0.2) \times 10^{26}$ molecules per second measured at 6.8 AU after adjusting each of their results for differences in fluorescence efficiencies and modeling (*12*). The agreement in the derived value of Q_{CN} among the three sets of spectroscopic observations made over a 6-week interval in 1995 imply that Hale-Bopp was in a quasi-steady state of production during the measurements.

Finally, we also examined the reflectance spectrum (*15*) of Hale-Bopp by extracting a spectrum of the comet centered on the nucleus and extending ± 26 arc sec ($\pm 1.25 \times 10^5$ km at the comet) into the coma. Our reflectance spectrum shows that the dust coma of Hale-Bopp is ~10% redder than the sun per 1000 Å over our entire spectral coverage consistent with previous reflectance spectra of Hale-Bopp (*3*).

REFERENCES AND NOTES

1. A. Hale and T. Bopp, *IAU Circular 6187* (1995).
2. Orbital elements by D. Green, *IAU Circular 6191* (1995).
3. A. Fitzsimmons and I. M. Cartwright, *Mon. Not. R. Astron. Soc.* **278**, L37 (1996).
4. In 1990, CN was detected in the coma of the enigmatic cometary-like object (2060) Chiron at $r_h = 11.3$

AU during an apparent outburst. S. J. Bus, M. F. A'Hearn, D. G. Schleicher, E. Bowell, *Science* **251**, 774 (1991).
5. Previously, the most distant detection of cometary CN emission was in the coma of P/Halley at r_h of 4.7 AU in February and March of 1985. S. Wyckoff, R. M. Wagner, P. A. Wehinger, D. G. Schleicher, M. C. Festou, *Nature* **316**, 241 (1985).
6. The Multiple Mirror Telescope Observatory, is a joint facility of the University of Arizona and the Smithsonian Institution. The spectra covered 3200 to 6700 Å at a dispersion of 1.2 Å pixel^{-1} and when combined with a 1-arc-sec-wide entrance slit our spectral resolution was 3.6 Å full-width at half-maximum (FWHM). The scale in the spatial direction was 0.6" pixel^{-1} or 2890 km pixel^{-1} at the comet. Due to other programs, the total length of the slit was constrained to be 75 arc sec or 3.6×10^5 km at the comet. Image motion tests at the end of the night through one telescope indicated that the seeing was 0.9-arc-sec FWHM. However, the combined beam of the ensemble of telescopes and spectrograph optics yielded stellar images 2 to 3 arc sec FWHM and 6 to 7 arc sec full-width at zero intensity so there was loss of light from the standard calibration stars through the 1-arc-sec-wide slit. The transparency of the sky was excellent during our observations.
7. R. M. Wagner, in *Astronomical CCD Observing and Reduction Techniques*, S. B. Howell, Ed., *Astron. Soc. Pac. Conference Series* **23**, 160 (1992).
8. R. M. Wagner, B. L. Lutz, S. Wyckoff, *Astrophys. J.* **322**, 544 (1987).
9. D. G. Schleicher, thesis, University of Maryland (1983).
10. M. F. A'Hearn, R. L. Millis, D. G. Schleicher, D. J. Osip, P. V. Birch, *Icarus* **118**, 223 (1995).
11. C. E. Randall, D. G. Schleicher, R. G. Rallou, D. J. Osip, *Bull. Am. Astron. Soc.* **24**, 1002 (1992); C. E. Randall and D. G. Schleicher, in preparation.
12. D. G. Schleicher, S. M. Lederer, R. L. Millis, T. L. Farnham, *Science* **275**, 1913 (1997).
13. M. Kleine, S. Wyckoff, P. A. Wehinger, B. A. Peterson, *Astrophys. J.* **436**, 885 (1994).
14. A. L. Cochran, *Bull. Am. Astron. Soc.* **28**, 1093 (1996); private communication.
15. The reflectance spectrum was derived by dividing the spectrum of the comet by the spectrum of the solar analog star and then normalized to unity at 5500 Å.
16. We thank the staff of the Multiple Mirror Telescope Observatory for their efforts which made these observations possible. This work was partially supported by NASA grants NAG5-2355 to The Ohio State University and NAGW-3884 to Lowell Observatory.

10 February 1997; accepted 6 March 1997

Diffusing-Wave Spectroscopy of Dynamics in a Three-Dimensional Granular Flow

Narayanan Menon and Douglas J. Durian

Diffusing-wave spectroscopy was used to measure the microscopic dynamics of grains in the interior of a three-dimensional flow of sand. The correlation functions show that minutely separated grains fly from collision to collision with large random velocities. On a time scale 10^3 to 10^4 times longer than the average time between collisions, the grains displayed slow, collective rearrangements, which, at the long-time limit, produced diffusive dynamics.

Sand dunes, grain silos, hourglasses, catalytic beds, filtration towers, river beds, ice fields, and many foods and building materials are granular systems (*1*). They consist of large numbers of randomly arranged, distinct, macroscopic grains that are too large to be moved by thermal energies but can be driven into flow by external forces. We do not have an understanding of the fluid state of a granular medium analogous to that for the macroscopic flow properties of a liquid. In a series of seminal papers, Bagnold (*2*) made the first efforts toward creating a phenomenological "fluid mechanics" for sand, identifying inertia of the grains and their collisions as significant elements in the dynamics. Since then there has been considerable theoretical effort (*3*) in formulating a continuum description of granular flows based on the kinetic theory of dense gases. However, in contrast to molecular fluids, kinetic energy in grain flows is irreversibly lost in the inelastic collisions of the grains. A further complication is that the scale of velocity fluctuations in the material (referred to as the "granular temperature") is nonthermal and has been difficult to measure, especially in three-dimensional (3D) flows (*4*). Also, recent computer simulations and theoretical work (*5*) show that 1D and 2D inelastic systems spontaneously form inhomogeneities that potentially restrict the applicability of hydrodynamic approaches to grain flow.

Department of Physics and Astronomy, University of California, Los Angeles, CA 90095–1547, USA.

We used diffusing-wave spectroscopy (DWS) (*6*) to probe the local, short-time dynamics of grains in a 3D gravity-driven flow and examine the physical basis of hydrodynamic models. DWS is a multiple–light-scattering technique that yields two-particle correlation functions at time intervals greater than 10^{-8} s and spatial separations greater than 1 Å. These capabilities are necessary because the collisional dynamics we studied are at time scales of 10^{-6} to 10^{-4} s and length scales of 0.01 to 1 μm. Because granular materials strongly scatter light, earlier experiments have chiefly studied quasi-2D flows (*7*) or highly diluted flows (where the short-time dynamics are collisional by construction). Experiments in dense flows (*8–10*) have been analyzed (*8*, *9*) with the assumptions that short-time dynamics are collisional and that the quantities of interest may be inferred from long-time, spatially averaged motions obtained by direct imaging of tracer beads.

The granular material we studied consisted of dry, cohesionless, monodisperse, smooth, spherical glass beads (*11*) 95 or 194 μm in diameter. The flow was gravity-driven (*12*) and confined to a vertical channel 30 cm high, 10 cm wide, and 0.3 to 1 cm thick (Fig. 1). Video and DWS measurements showed that spatial gradients in all three dimensions were small and that the flow field everywhere in the channel was characterized by a single average flow velocity V_f. We varied V_f from 0.03 to 3 cm/s by changing the mesh size at the bottom of the channel. The arrangement of the beads in flow showed no evidence of density inhomogeneities or crystalline packing.

For DWS measurements, we illuminated the sample with an Ar^+ laser of 488- or 514-nm wavelength and 3-mm beam waist. Incident photons were multiply scattered by the glass beads, performed random walks through the sample, and interfered, producing a speckled pattern. Grain motions caused this pattern to fluctuate, decorrelating the intensity measured at the detector. To infer the dependence of the dynamics of the beads on time τ from the autocorrelation function $g_1(\tau)$, we described photon transport as a random walk through the medium with a step length l^* and an absorption length l_A (which were determined by measuring the fraction of light transmitted through the sample as a function of its thickness). For example, the normalized electric-field autocorrelation function in transmission (Fig. 2A) is $g_1(\tau) \approx \exp[-(L/l^*)^2 k^2 \langle \Delta r^2(\tau) \rangle]$, where L is the sample thickness, $\langle \Delta r^2(\tau) \rangle$ is the mean-squared displacement of the scatterers, k is the wave vector of light in the medium, and the factor $(L/$

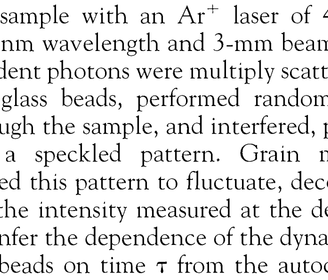

Fig. 1. Side view of the flow and light-scattering geometry.